# Induced-Fission Imaging of Nuclear Material*

Paul A. Hausladen, Matthew A. Blackston, James A. Mullens, Seth McConchie, John T. Mihalczo, Philip R. Bingham, M. Nance Ericson, Lorenzo Fabris

*Oak Ridge National Laboratory, 1 Bethel Valley Road, Oak Ridge, TN, 37831-6010*

**ABSTRACT**

This paper presents initial results from development of the induced-fission imaging technique, which can be used for the purpose of measuring or verifying the distribution of fissionable material in an unopened container. The technique is based on stimulating fissions in nuclear material with 14 MeV neutrons from an associated-particle deuterium-tritium (D-T) generator and counting the subsequent induced fast fission neutrons with an array of fast organic scintillation detectors. For each source neutron incident on the container, the neutron creation time and initial trajectory are known from detection of the associated alpha particle of the d + t → α + n reaction. Many induced fissions will lie along (or near) the interrogating neutron path, allowing an image of the spatial distribution of prompt induced fissions, and thereby fissionable material, to be constructed. A variety of induced-fission imaging measurements have been performed at Oak Ridge National Laboratory with a portable, low-dose D-T generator, including single-view radiographic measurements and three-dimensional tomographic measurements. Results from these measurements will be presented along with the neutron transmission images that have been performed simultaneously. This new capability may have applications to a number of areas in which there may be a need to confirm the presence or configuration of nuclear materials, such as nuclear material control and accountability, quality assurance, treaty confirmation, or homeland security applications.

## Introduction

Neutron counting has long been used to perform bulk characterization of nuclear material. Coincidence or multiplicity techniques are often used to isolate or characterize the fission component of neutron emanations, and for materials where the intrinsic fission rate is low, it is common to perform the measurements following increasing the fission rate via some sort of active interrogation [1–3]. In the present work, fissions are induced via steady-state interrogation with a deuterium-tritium (D-T) neutron source. The fission response is measured during interrogation and is associated with the initial path of the interrogating 14 MeV neutron through the inspected object. The initial trajectory of each source neutron is known from detection of the associated alpha particle of the d + t → α + n reaction, and many induced fissions lie along or near the interrogating neutron path. Because the induced-fission signal can be associated with lines of response through the object, image reconstruction techniques can be applied to form an image of the induced-fission probability per unit length multiplied by a property of the fission chain that depends on the observable, such as the average number of neutrons or average number of neutron pairs, for each volume element of the image. Neutrons that do not interact in the inspected object can be used to determine the total probability of interacting per unit length. By measuring on a voxel-by-voxel basis, sensitivity to anomalies and ease of interpretation can be increased compared to bulk analysis, particularly for inspected objects that are inhomogeneous or whose geometry is not known.

The components of a system capable of performing combined transmission and induced-fission imaging are indicated schematically in Figure 1. The D-T neutron generator, where interrogating 14 MeV neutrons are created by the $d + t \rightarrow \alpha + n$ reaction, is shown to the left. As indicated in the figure, each

neutron has an associated alpha particle traveling in the opposite direction. The time and position of each alpha particle incident on the alpha-particle detector are recorded, which determine the time and direction of the interrogating 14 MeV neutron incident on the inspected object, up to the uncertainty in direction associated with the alpha-particle detector resolution and finite source size. In the figure the neutron generator is shown expanded in order to be able to indicate its internal functioning; the actual D-T generator fits inside a 7.5 cm diameter tube, while the inspected object might typically be a 55 gal drum. Neutrons from the D-T generator traverse the inspected object, where they are subjected to interactions with nuclei in the inspected object in proportion to the cross section for that interaction and the number density of nuclei in the object. These interactions consist of elastic and inelastic scattering as well as reactions such as neutron knockout and neutron-induced fission. A combination of transmitted, scattered, and reaction-product neutrons (including induced-fission neutrons) reaches the fast organic scintillator detector array, shown to the right in Figure 1, where neutron times and positions are recorded.

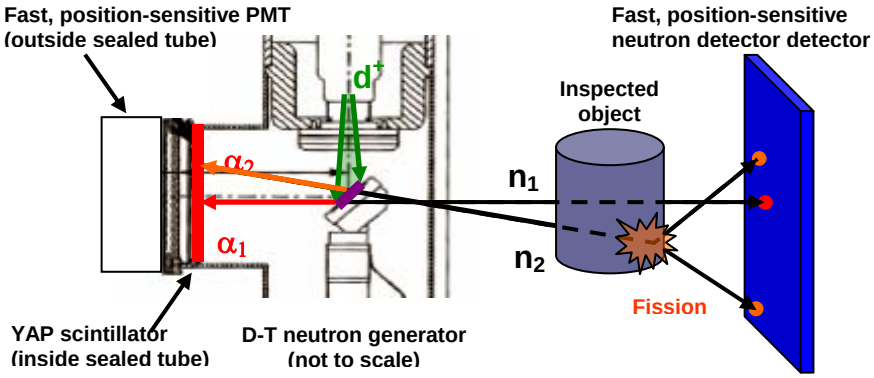


Figure 1: Schematic diagram of a combined transmission and induced-fission imaging system based on a D-T neutron generator with an associated alpha-particle detector. The D-T generator is expanded in this view to show the alpha particle coincident with each interrogating neutron.

Transmission neutrons that traverse the inspected object can be identified because they are detected at the appropriate time and location as determined by the associated alpha particle. Prompt fission and other reaction product neutrons are separated by time of flight from the transmission neutrons, so multiplicity counting with fast organic neutron detectors is possible in the tens of nanoseconds after transmitted neutrons arrive at the neutron detector. The multiplicity counting in a time window following each alpha particle serves to associate the induced-fission signal with each direction through the inspected object.

**Contrast for Fission**

The 14 MeV neutrons used for interrogation are both higher in energy than fission-spectrum neutrons and above the neutron separation energy of most nuclei. This leaves the possibility that down-scattered 14 MeV neutrons or reaction-product neutrons originating from reactions other than fission result in one or more neutrons detected at times of flight consistent with the timing window in which fission neutrons are expected. As a result, the number of late-arriving neutrons and neutron multiples from benign materials as well as actinides were estimated from compiled cross sections in the ENDF/B-VII evaluated nuclear data files by considering all evaluated cross sections for neutrons leading to a variety of single or multiple neutron states. For example, a nuclide-by-nuclide estimate of the number of neutrons arriving later than transmitted neutrons was made by summing the cross sections of all reactions leading to single-neutron output states where the neutron energy differs significantly from its original energy, including (n,nγ), (n,np), (n,nd), (n,nt), (n,n$^3$He), (n,nα), (n,n2p), (n,npα), (n,n2α), (n,nd2α), (n,nt2α), and (n,n3α) for each nuclide. Likewise, the 2n reaction channels (n,2n), (n,2np), (n,2nd), (n,2nα), and (n,2n2α); the 3n channels (n,3n) and (n,3nα); the 4n channel (n,4n); and the fission reaction (n,fiss) channel cross sections were weighted by the number of neutrons released in the reaction and summed. The resultant cross-section weighted number of neutrons induced by 14 MeV neutrons incident on all nuclides is shown in the leftmost plot of Figure 2. The ordinate of the plot has units of neutron·barns, so that either a five barn cross section yielding one neutron or a one barn cross section yielding five neutrons would equal 5 on this plot. Note that all elements produce late-arriving neutrons, approximately in proportion to the number of

neutrons in the nucleus, until the turn-on of the fission cross section clearly delineates the actinides from lighter elements. However, it is also worth noting that the contrast between non-multiplying quantities of fissionable nuclides and heavy elements such as lead is only about a factor of two, and that sensitivity to late neutrons from all the nuclides will scale together with the efficiency of the neutron-detector array.

The number of neutron pairs is more indicative of fission, but nonzero cross sections for multiple-neutron exit channels in almost all elements means that late neutron pairs are also not unambiguous, and production in benign materials must be accounted for in analysis. However, the number of distinct ways to make neutron pairs increases rapidly with the number of neutrons, so that while three neutrons can give 3 distinct pairs, ten neutrons can make 45 distinct pairs. This way, despite the ability to get neutron pairs from neutron knockout reactions off most nuclides, the larger neutron multiplicities from fission reactions are heavily favored. The rapid increase of pairs with the number of neutrons also gives sensitivity that is a strong function of multiplication because multiplying assemblies have nonzero probabilities of large numbers of neutrons emitted in fission chains.

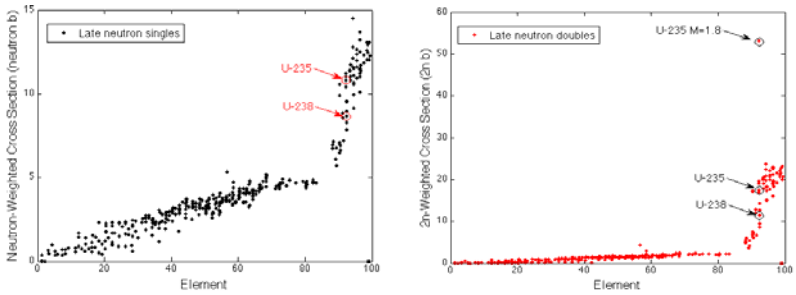


Figure 2: Contrast from (left) late neutron singles and (right) late neutron doubles from nuclear data. All exit channels including neutrons in the evaluated nuclear data files ENDF B/VII were considered.

The estimated contrast based on the pair-weighted cross sections for producing multiple neutrons can be seen to the right in Figure 2. Note that the contrast between fissionable nuclides and heavy nuclides such as lead increases from the approximate factor of two for the neutron singles observable to nearly a factor of ten for the observable of neutron pairs. The single point labeled "U-235 M=1.8" gives an indication of the effect of multiplication on the increase in the number of neutron pairs associated with multiplication, in this case for the modest multiplication of 1.8 expected for a standard storage casting with a height of 15 cm, outer diameter of 12.7 cm, inner diameter of 8.89 cm, and material enriched to 93% $^{235}$U. While it is apparent that neutron pairs give increased contrast for fission, the increased contrast comes at the price of reduced efficiency because sensitivity to late-neutron pairs scales like the square of the neutron detector efficiency and, contrary to the assumptions of point-kinetic theories, there is not a single efficiency for the detection of emitted neutrons that can be used to characterize the interrogation volume. Rather, the pixel-by-pixel value of the efficiency may vary by an order of magnitude or more across a volume and significantly change the sensitivity to neutron pairs based on the location of the material or the location of the fission within the material.

To show the contrast between multiplying, fissionable, and benign materials, an example induced-multiplicity measurement was simulated and is shown in Figure 3(a). The simulation was performed with version 4.9 of the Geant4 toolkit using the Lawrence Livermore National Laboratory library for neutron and gamma-ray emission from fission. In this simulation the inspected object consists of three storage castings of high-atomic-number material, in this case W, $^{nat}$U, and highly enriched uranium (HEU). The D-T source is indicated by the cylinder from which neutron trajectories (green) are emanating, and the detector consists of a five-detector-high by seven-detector-wide panel of individual fast-neutron detectors. Detector counts as a function of time after the D-T neutron leaves the source are shown for neutrons incident on each of the storage castings in Figure 3(b). The late window in which induced-fission neutrons are counted is also indicated. In Figure 3(c), histograms of the number of occurrences of each number of detected neutrons are shown for neutrons incident on each of the storage castings. When they are normalized by the initial source neutrons, these histograms correspond to the detected neutrons per source neutron distributions that could be fit to a point-kinetic calculation of probability of first fission,

multiplication, and detection efficiency. The distributions of detected neutrons in the fission window can be measured for each incident neutron direction and summarized as an image. Panels (e) through (g) of Figure 3, for example, summarize a number of simple properties of the measured neutron chain as an image, including the number of neutrons in the fission window in (e), the number of pairs of neutrons in the fission window in (f), and the ratio of pairs to singles in (g). All of these images show contrast for HEU that was not present in the transmission image of panel (d). The ratio of neutron pairs to neutrons of panel (g) is referred to as the Feynman variance and is a common way to measure the length of fission chains. The images of Figure 3 are useful to indicate a number of effects. First, there is contrast for fission, and this contrast is largely associated with the initial direction. Second, interaction between distinct volumes is evident. For example, in panel (f), comparison of the left and right side of the $^{nat}$U casting indicates that either neutrons incident on the $^{nat}$U casting scatter into the HEU for increased likelihood of fission, or induced fissions on the HEU side of the $^{nat}$U casting have an increased likelihood of longer chains, or both.

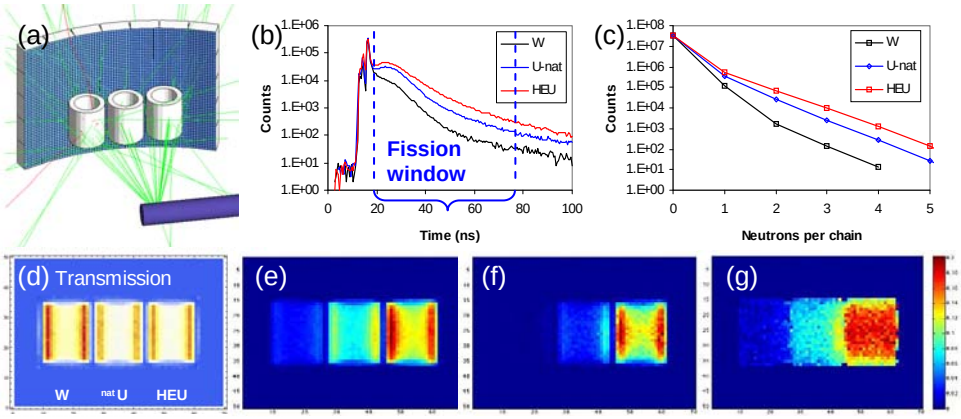


Figure 3: Simulated induced-multiplicity measurement showing (a) the measurement geometry with three storage castings constructed of high-atomic-number materials W, $^{nat}$U, and HEU; (b) the time distribution of counts after the D-T neutron leaves the source, where the time window in which fission neutrons are counted is indicated; and (c) the number of counts in the fission window. The images show (d) D-T neutron transmission through the castings, (e) the number of neutrons in the fission window, (f) the number of neutron pairs in the fission window, and (g) the Feynman variance for each incident neutron direction.

Last of all, it is evident that there is some signal level for late neutrons from the W casting. Some of this signal originates from the neutrons scattering into neighboring fissionable or fissile volumes, but some of the signal originates in the W casting itself.

**Induced-Fission Tomography**

Induced-fission tomography is best explained in analogy to transmission imaging. Transmission imaging is performed when no interactions occur and the transmitted neutron is detected on the other side of the object. The transmitted neutrons decrease with thickness of the object as $e^{-\mu x}$, where $\mu$ is the attenuation coefficient. The attenuation coefficient is the product of the total cross section and the number density and has units of inverse length. Its product with a short length $\mu\Delta x$ is the probability that a neutron will interact in the length $\Delta x$. Its inverse $1/\mu$ is known as the attenuation length and corresponds to the length of material that reduces the number of uncollided neutrons along a trajectory by $1/e$. A transmission radiograph gives an image of $\mu x$ along each path through the object and is extracted from measured data by taking the logarithm of the ratio of the number of neutrons with and without the object present. In instances in which a number of views through an object can be combined, a cross-sectional, or tomographic, reconstruction of the transmission data gives the value of the attenuation coefficient $\mu$ for each pixel in a slice through the object. Such an image has contrast because different materials have different values of $\mu$ originating either from different total nuclear cross sections or different number densities of nuclei.

Similar to transmission imaging, the product of the cross section for fission and the number density of fissionable nuclei gives the attenuation coefficient for fission reactions, $\mu_f$, which is possible for

interactions involving actinide elements. The product of the attenuation coefficient for fission and a short length $\mu_f \Delta x$ is the probability that a neutron induces fission in the length $\Delta x$. Unlike the total interaction probability, the number of induced fissions cannot be measured directly. However, the number of induced neutrons can be measured and can be measured as a distribution in number and in time. Also unlike the total interaction probability, the number of induced neutrons is determined by both nuclear data and the geometry of the object as a whole. The combination of these factors determines the average length of fission chains initiated within a particular voxel of the object. The image contrast of an induced-fission radiograph can consist of the product of fission probability per unit length and length ($\mu_f x$) times some property of the neutron chain length, such as the average number of neutrons in a chain, for each path through the object. In instances in which a number of views through an object can be combined, a tomographic reconstruction will give the value of the attenuation coefficient for fission $\mu_f$ times some property of the neutron chain length (determined by the observable) for each pixel in a slice through the object. Observables consisting of the number of neutrons and the number of neutron pairs in the fission window are considered in the present work.

Consider a single view of an object containing fissionable material being imaged using fast neutrons. A schematic diagram of such an object (consisting of an HEU storage casting in a lead box along with some polyethylene and an iron piece) is shown in Figure 4.

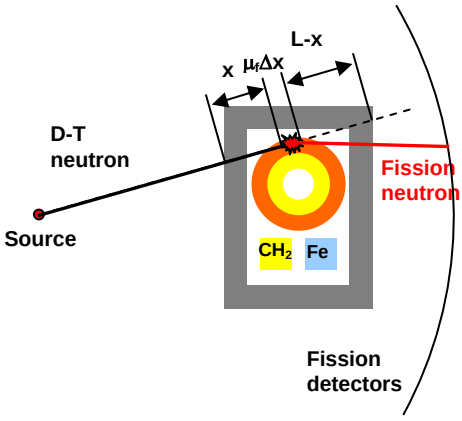


Figure 4: Schematic diagram of induced-fission imaging of an object using the number of neutrons detected in the "fission window."

In a volume element of the fissionable material that has an attenuation coefficient due to fission $\mu_f$ and size $\Delta x$, the probability that an interrogating neutron will fission a nucleus in the length $\Delta x$ is $\mu_f \Delta x$. The average number of neutrons released by the fission chain can be written $\langle \nu \rangle_{chain}$, yielding an average number of neutrons produced per fast neutron incident on the interval $\Delta x$ of $\mu_f \Delta x \langle \nu \rangle_{chain}$. The number of neutrons $\langle \nu \rangle_{chain}$ can be related to the probability distribution of neutrons in the fission chain $P(\nu)$ by point-kinetic theory to the multiplication of the object (that encodes the dependence of the fission chain length on the geometry of the object as a whole), $M$; the average number of neutrons released by a 14 MeV neutron induced fission, $\langle \nu \rangle_{14MeV}$; and the number of neutrons released by fission-spectrum neutron-induced fission, $\langle \nu \rangle$.

$$\langle \nu \rangle_{chain} = \sum \nu P(\nu) = \langle \nu \rangle_{14MeV} \left( M - \frac{1}{\langle \nu \rangle} (M - 1) \right)$$

The number of neutrons generated in a volume element per fast neutron incident on it needs be related to the measured number of neutrons detected in the fission window per source neutron initially heading in that direction. In Figure 4 the number of incident neutrons are attenuated over the length $x$ in getting to the volume element in which fission takes place, and provided the fission neutron path is not too different from the original neutron trajectory, the emitted fission neutrons are attenuated over the length $L$-$x$ before reaching the detectors. The additional fission neutrons at the detectors $\Delta n$ originating from the length $\Delta x$ can then be written

$$\Delta n \approx N(\mu_f \langle \nu \rangle_{chain} \Delta x)(e^{-\mu x})(e^{-\mu(L-x)}) = Ne^{-\mu L}(\mu_f \langle \nu \rangle_{chain} \Delta x),$$

where $N$ is the incident number of neutrons, $e^{-\mu x}$ is the attenuation of source neutrons on the way to the volume element with fissionable material, $\mu_f \langle \nu \rangle_{chain} \Delta x$ is the average number of neutrons produced in the volume element with length Δx, and $e^{-\mu(L-x)}$ is the attenuation of fission neutrons from the volume element to the detectors. Provided the attenuation coefficient for 14 MeV neutrons on the way in is close to the attenuation coefficient for fission-spectrum neutrons on the way out, the exponents add to give a factor that depends on only the total attenuation of the object $e^{-\mu L}$. For simplicity of exposition, the attenuation of the object has been written as a single attenuation coefficient, although more correctly it is the sum over each path length of each material in the object. In addition, the effective attenuation coefficient of interest is one that properly characterizes the drop in the population of fast neutrons that can cause fission with distance into the object. In most cases this effective cross section excludes the elastic scattering cross section because elastic scatters off all elements except hydrogen essentially do not change the energy of the scattered neutron, are forward peaked so they change the neutron energy very little, and typically constitute about 50% of the total cross section. The expected effective cross section for the drop in the population of fast neutrons that can cause fission is therefore less than half the total cross section. The total number of induced fission-spectrum neutrons $n$ per source neutron that emerges from the far side of the object $Ne^{-\mu L}$ is therefore the sum of probabilities for producing neutrons in each volume element along a ray from the source to detectors:

$$\sum \mu_f \langle \nu \rangle_{chain} \Delta x = \frac{n}{Ne^{-\mu L}}.$$

Because the contribution of each volume element is now (at least approximately) a linear sum, tomographic reconstruction of induced-fission singles can be performed similarly to conventional transmission computed tomography, such as by filtered back projection. The value that will be reconstructed for each pixel will be $\mu_f \langle \nu \rangle_{chain}$, which for depleted uranium metal is 0.24 neutrons $cm^{-1}$ from fission and an additional 0.18 neutrons $cm^{-1}$ from other reactions such as (n,2n) and (n,3n) for a total of 0.42 neutrons $cm^{-1}$. For a thin target of HEU metal, there will be 0.44 neutrons $cm^{-1}$ from fission and an additional 0.08 neutrons $cm^{-1}$from other reactions for a total of 0.52 neutrons $cm^{-1}$. For HEU metal in the storage casting configuration, the multiplication of the object boosts the neutron yield from fission to 0.65 neutrons $cm^{-1}$, for a total of 0.73 neutrons $cm^{-1}$, nearly twice that of depleted uranium (DU). From Figure 2, it can be seen that other high-atomic-number nuclides like lead have the highest non-actinide cross sections for neutron production, so comparison to a material like lead is useful. For lead the number of neutrons produced is 0.16 neutrons $cm^{-1}$, less than half the value for DU. For correct quantitative reconstructed values of neutrons $cm^{-1}$, a number of factors need to be taken into account, including the different neutron detector efficiencies for 14 MeV and fission spectrum neutrons and the solid angle of the neutron detector array for detection of the isotropic fission neutrons. If the measured object is placed near enough to the neutron detectors that solid angle differences from different points in the object are substantial and the contribution of detected fission neutrons that have very different paths from the original interrogating neutron path are also substantial, then the approximate linearity presumed above will break down. Under such circumstances an iterative approach to reconstruction in which attenuations to and from each volume element of the inspected object and solid angles subtended by the detectors from each volume element can be calculated explicitly as required.

Now consider the object shown earlier in Figure 4, but where the observable is the detection of two neutrons. The additional fission neutron pairs at the detectors $\Delta n_2$ from the volume element of length $\Delta x$ can then be written as

$$\Delta n_2 \approx N(\mu_f \langle \nu_2 \rangle_{chain} \Delta x)(e^{-\mu x})(e^{-2\mu(L-x)}) = Ne^{-\mu(2L-x)}(\mu_f \langle \nu_2 \rangle_{chain} \Delta x),$$

where $N$ is the incident number of neutrons, $e^{-\mu x}$ is the attenuation of source neutrons on the way to the volume element with fissionable material, $\mu_f \langle \nu_2 \rangle_{chain} \Delta x$ is the average number of neutron pairs produced in a volume element with length Δx, and $e^{-2\mu(L-x)}$ is the probability of getting two fission neutrons from the volume element to the detectors. Note that in the instance of late doubles, the number of neutron pairs $\Delta n_2$ contributed by each length $\Delta x$ along the interrogating neutron trajectory cannot be summed without modification by the term $e^{-2\mu(L-x)}$ that is explicitly nonlinear in $x$. The physical interpretation of this statement is that the same volume element of fissionable material placed at different locations along the

path through the inspected object would produce different measured contributions of neutron pairs. Under such circumstances an iterative approach to reconstruction is necessary. In such an approach, attenuations to and from each volume element of the inspected object and solid angles subtended by the detectors from each volume element need to be calculated explicitly. The outcome of the late-doubles reconstruction is to associate the probability per unit length of producing a pair of neutrons, $\mu_f \langle \nu_2 \rangle_{chain}$, with each pixel of the image. The actual value of this number for DU metal is 0.55 neutron pairs $cm^{-1}$. For a thin target of HEU metal, the value will be 0.84 neutron pairs $cm^{-1}$, while for HEU metal in the storage casting configuration enriched to 93% $^{235}U$ (multiplication 1.8), the multiplication of the object boosts the yield to 2.57 neutron pairs $cm^{-1}$, nearly five times the value for DU. For the high-atomic-number comparison material of lead, the number of neutron pairs produced is 0.07 $cm^{-1}$, about 1/7th the value of DU and 1/35th the value of the multiplying assembly of HEU.

**Measurements**

The Advanced Portable Neutron Imaging System (APNIS) was developed at Oak Ridge National Laboratory to perform transmission and induced-fission imaging with 14 MeV neutrons. The imaging system consists of a Thermo-Fisher Scientific API120 D-T neutron generator that has an embedded alpha-particle detector. The alpha-particle detector consists of a 50 mm diameter by 0.5 mm thick Cerium-doped yttrium aluminum perovskite (YAP:Ce ) scintillator that is mounted 57 mm from the target position of the mixed D-T beam. The scintillator has a 1 μm coating of aluminum that acts to ground the detector, stop the scattered beam before it reaches the active volume of the scintillator, and aid in light collection of the scintillation light while shielding the photomultiplier from direct illumination by light produced from target ionization. The scintillator is viewed through a Schott-type 75C fiber-optic faceplate by a Hamamatsu H8500 64-pixel photomultiplier tube (PMT) fronted by a custom fused-silica light guide. The faceplate material was chosen for its adequate transmission of the near-ultraviolet scintillation light from YAP:Ce. The light guide is segmented into a 32 × 16 array of 1.5 × 1.5 mm pixels that linearizes and discretizes the position response of the detector. The light guide covers the vertically-central half the active area of the PMT. The neutrons coincident with the detected alpha particles illuminate an 8 × 4 array of neutron detectors. The neutron detectors each consist of a 10.4 cm × 10.4 cm × 5 cm block of fast plastic scintillator segmented into 100 pixels that are read by four photomultipliers whose shared response determines the pixel of interaction. The fine segmentation of the neutron detectors is primarily useful for transmission imaging, but the amount of solid angle subtended by the array allows it to be used for the detection of induced-fission neutrons as well. Detectors are read out and coincidence logic performed by commercial positron emission tomography hardware from Siemens. A picture of the imaging system, with the D-T generator on the left side and the neutron detector array on the right, can be seen in Figure 5.

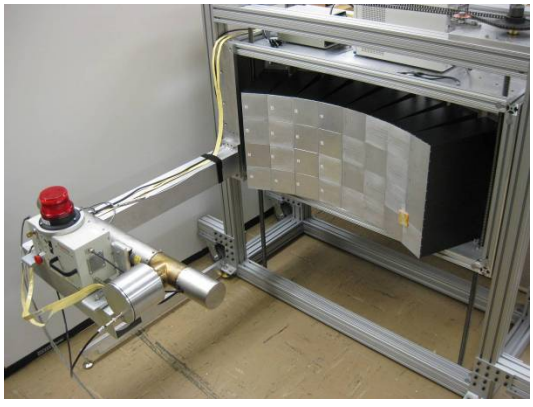

Figure 5: The APNIS imaging system. The D-T neutron generator with associated alpha-particle detector is on the left side, and the imaging neutron detector array is on the right.

First transmission and induced-fission measurements with the system were performed using an annular DU storage casting in an annular can together with a lead brick and a steel brick. The combined object was centered on a turntable whose center of rotation was located halfway between the D-T neutron source

and the neutron detectors. A photograph of the object with the neutron detector array in view is shown to the left in Figure 6. Transmission and induced-fission projection measurements were performed every 10 degrees for a total of 36 angles. Each projection was measured for 2.5 min for a total of 90 min with a neutron output from the D-T generator of $8.6 \times 10^6$ neutrons $s^{-1}$ into $4\pi$. A single transmission projection of the object is shown on the right side of Figure 6.

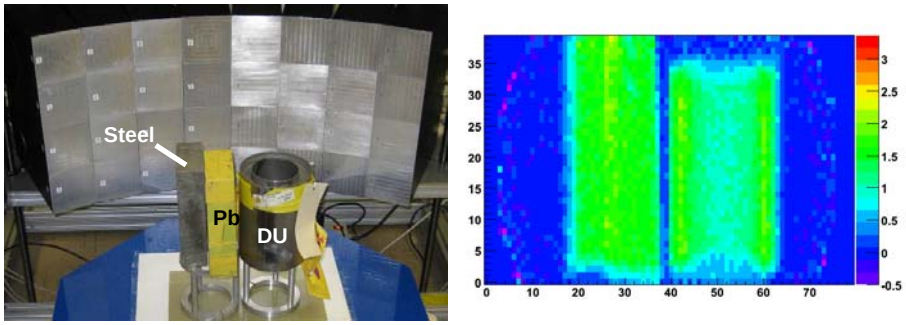


Figure 6: Induced-fission measurement of a DU casting accompanied by a lead brick and a steel brick.

Transmission reconstruction

The central horizontal slices through each of the 36 transmission images were assembled into a sinogram, and the sinogram was used as input to an iterative code that was used to reconstruct the attenuation coefficients of a cross-sectional slice through the object. The measured sinogram, reconstructed sinogram, and reconstructed image are shown in Figure 7.

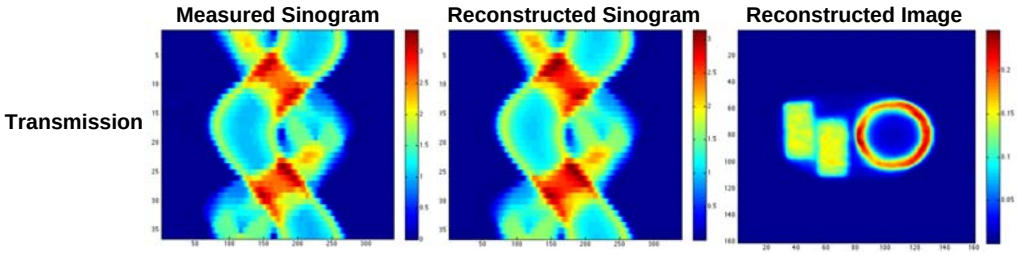


Figure 7: Measurement and tomographic reconstruction (for transmission) of DU, lead, and steel object.

Induced neutron singles reconstruction

A tomographic reconstruction was also performed using induced-fission neutron singles. The measurement observable in this case consists of the number of late neutrons detected per source neutron that transmitted through the object and was calculated for each alpha-detector pixel for each projection. While for the transmission image, the neutron path through the object is inferred from the neutron pixel that was hit, for induced-reaction images the neutron path through the object is inferred from the coincident alpha pixel. Each alpha-particle pixel defines a ray through the object, but because of the proximity of the alpha-particle detector to the D-T target where neutrons are produced, the finite size of the target contributes an uncertainty of 5 degrees in the initial neutron direction. Consequently, the induced-reaction images are less well resolved than transmission images. The measured induced neutron singles sinogram can be seen in Figure 8, along with the reconstructed sinogram and reconstructed image.

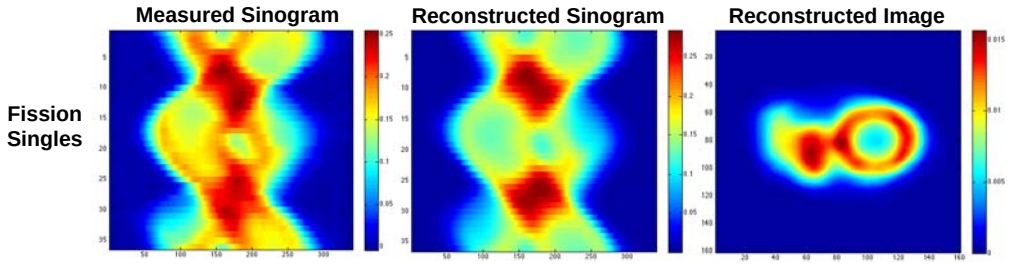


Figure 8: Measured induced neutron singles sinogram, reconstructed sinogram, and reconstructed induced neutron singles image. Because of the lack of resolution for the initial neutron direction with the 5 mm target spot inside the D-T generator, the contrast between DU and lead is not apparent.

Note that the lack of resolution makes it difficult to see the contrast between DU and lead, even though the estimate from compiled nuclear data gives 0.42 neutrons $cm^{-1}$ for uranium and 0.16 neutrons $cm^{-1}$ for lead. This lessened apparent contrast is because the 5 cm thickness of the lead block is much larger than the 1.9 cm thickness of the uranium casting. The actual contrast can be recovered by insisting that the origin of induced neutrons must be within objects that have neutron attenuation. This is accomplished in the reconstruction in practice by using a starting guess whose nonzero points are limited to those points in the transmission image that are at least 0.2 times the maximum value. Then, in the forward-projection step, the calculated forward projection is smeared by the known width of the coincident neutron cone from a single alpha-detector pixel. The resulting constrained reconstruction is shown in Figure 9 along with the transmission reconstruction and unconstrained induced neutron singles reconstruction for comparison. This reconstruction now shows contrast between DU and lead.

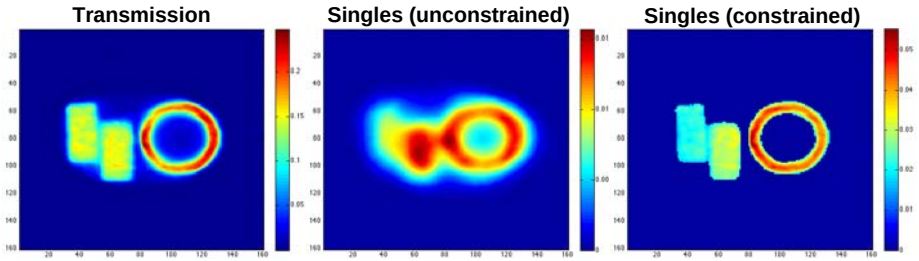


Figure 9: Induced neutron singles reconstruction constrained to the transmission geometry (right) with transmission (left) and unconstrained induced neutron singles (center) for comparison.

In general, constraints on the geometry may be less useful than shown in the present example because the objects in this example are separated from each other rather than closely abutting. In the latter case, the inherent resolution of the initial neutron direction will be a limitation. Cases with close-fitting shielding will be examined in the future.

Induced neutron doubles reconstruction

A tomographic reconstruction was performed using induced neutron doubles. The doubles reconstruction explicitly uses the reconstructed transmission image, not just to identify locations in which fission density is allowed, but also to compute the attenuation of neutrons from the source to each volume element of the object containing a nonzero attenuation coefficient and from each of those volume elements to the neutron detectors. The computed combined probability of getting to and from all points in the inspection volume for projections at 0, 90, 180, and 270 degrees is shown in Figure 10. Note that in all cases the area of highest probability of generating a detected two-neutron event is nearest the detectors.

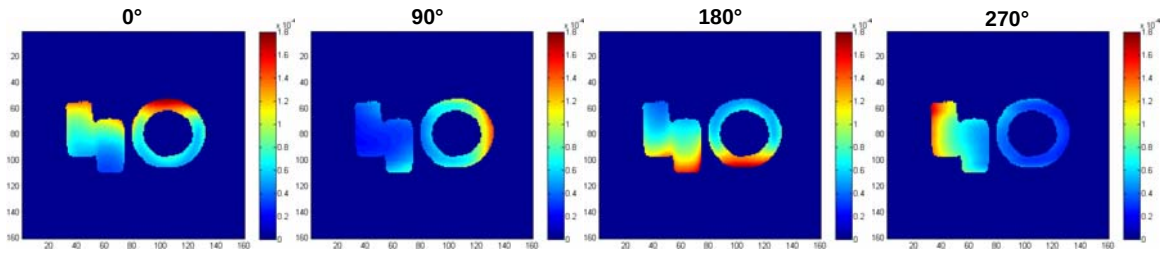


Figure 10: Calculated probability of a source neutron reaching and two neutrons being detected from each volume element of the transmission image.

For the reconstruction of induced neutron doubles, the guessed distribution starts with the transmission image itself, and the forward calculation to get the calculated sinogram uses the calculated probability mapping for each angle. The resulting calculated projection is then convolved with the known directional resolution for the interrogating neutron direction. The measured and calculated sinograms for the induced neutron doubles events are shown in Figure 11 along with the reconstructed induced-fission image. Note the excellent contrast between DU and either lead or steel in the induced-doubles image. Note also that a uranium casting enriched to 93% $^{235}$U is predicted to have approximately five times the number of induced neutron doubles as DU, in part because of a higher fission cross section and in part because of the multiplying nature of the enriched assembly.

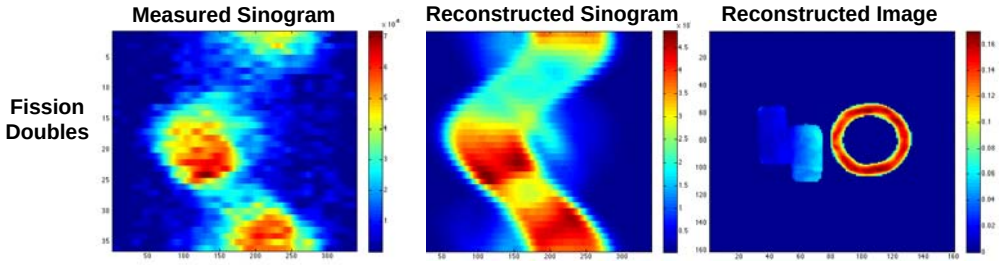


Figure 11: Induced neutron doubles measured sinogram, calculated sinogram, and reconstructed image.

## Conclusions

The present work has developed the new technique of combined neutron transmission and induced-fission imaging using associated-particle techniques and a D-T neutron generator. For this form of induced-emission computed tomography, neutron observables such as number of neutrons or neutron pairs produced per centimeter have been related to physical quantities associated with particular volume elements, such as the cross section for fission, as well as bulk properties of an object, such as the multiplication. An iterative reconstruction code has been developed to perform transmission and induced-neutron reconstruction. Last of all, experimental data have been reconstructed to demonstrate tomographic reconstruction of neutron production probabilities within an object and show contrast for DU, with much better contrast expected for multiplying assemblies of enriched uranium.

## References

1. C. L. Hollas, C. Goulding, and W. Myers, "Determination of neutron multiplication of subcritical HEU systems using delayed neutrons," *Nuclear Instruments and Methods in Physics Research A* **543**, 559–569 (2005).
2. C. E. Moss et al., "Comparison of Active Interrogation Techniques," *IEEE Transactions on Nuclear Science* **53**(4), 2242–2246 (2006).
3. M. Agelou et al., "Photofission tomography of nuclear waste packages," *IEEE Nuclear Science Symposium Conference Record*, 801–804 (2007).